DALHOUSIE UNIVERSITY

Experiments and Nonlinear Analysis of the Impact Behavior of Sandwich Panels Constructed with Flax Fibre-Reinforced Polymer Faces and Foam Cores

Dillon Betts [a], Pedram Sadeghian [a], and Amir Fam [b]

[a] Department of Civil and Resource Engineering, Dalhousie University, 1360 Barrington Street, Halifax, NS, B3H 4R2, Canada

[b] Department of Civil Engineering, Queen's University, Kingston, ON, K7L 3N6, Canada

ABSTRACT: As the effects of climate change become more apparent, it is necessary that environmental impact is considered in every aspect of our society, including the design of new infrastructure. The use of natural materials for building construction is one way to improve the sustainability of infrastructure and therefore it is important that the behavior of structures made with natural materials be investigated extensively and well understood. In this study, the performance of sandwich panels constructed with flax fibre-reinforced polymer (FFRP) faces and foam cores under impact loading is studied experimentally and analytically. The parameters of the tests were facing thickness (1, 2 and 3 layers of flax fabric) and core density (32, 64 and 96 kg/m^3). Each specimen was 1220 mm long, 152 mm wide and approximately 80 mm thick and was tested by a 10.41 kg drop weight impact at mid-span. Each specimen was tested multiple times starting at a drop height of 100 mm and increasing the height by 100 mm for each subsequent test until ultimate failure. The results indicate that the ultimate impact energy increases with both core density and face thickness. The four main failure modes observed were: compression face crushing, compression face wrinkling, core shear and tension face rupture. The failure modes observed generally matched those observed during similar quasi-static testing. Additionally, a nonlinear incremental iterative model (NIIM) was developed based on the conservation of energy during an impact event and the nonlinear mechanical

behavior of both the FFRP faces and foam cores. This novel model accurately predicts the total deflection and face strains based on the energy of an impact.

KEYWORDS: Sandwich; Composite; Flax; Bio-based; Impact; Nonlinear.

DOI: https://doi.org/10.1177/1099636220925073

1. INTRODUCTION

As the need for environmental consciousness increases, it is necessary to have sustainable building material options to replace or supplement conventional building materials. One method of making infrastructure more sustainable is the use of natural materials, such as plant fibres in fibre-reinforced polymer (FRP) composites. Numerous types of plant fibres have been researched for this purpose and one notable fibre is flax. Flax is readily available and has been shown to exhibit relatively high strength and stiffness when compared to other types of natural fibres [1].

A structural element for which natural FRPs can be used is the sandwich panel. Sandwich panels are often employed when a light weight and/or insulated structure is required. These panels are made up of strong thin faces separated by a weaker, lightweight core which increases the moment of inertia and improves the flexural rigidity of the structure [2]. Sandwich panel faces are often made of synthetic FRPs, such as glass or carbon FRPs, due to their relatively high strength and stiffness. Though weaker than traditional synthetic FRPs, flax FRPs (FFRPs) have been shown to have a lower embodied energy [3] and are therefore considered to be a more environmentally friendly. As the weak core material often dictates failure in sandwich panels, high performance FRPs are typically underutilized and FFRPs can be efficiently used as a sustainable replacement for synthetic FRPs for these structures [4–6]. Sandwich panels made with foam cores and FFRP faces have recently been studied under axial [7] and flexural loading [6, 8].

Sandwich panels are regularly used as a part of building envelopes. As these structures can be subjected to impacts from flying debris during high wind events, it is important to understand their behavior under low velocity impact loading. The low-velocity impact behavior of composite plates [9–11] and sandwich panels with synthetic faces [12–18] has been investigated. Abrate [19] and others [20–22] have presented a number of techniques for modelling synthetic FRP sandwich structures. Failure mode maps have been developed to predict the failure of these panels under dynamic loading [23, 24]. A sophisticated method of optimising properties of synthetic FRP sandwich panels for impact loading based on a genetic algorithm has also been developed [25]. Additionally, numerous studies have been completed on the modelling of sandwich structures under impact loads using the finite element method [26–33]. Some studies have also been performed on natural fiber sandwich panels under impact [34, 35], however, there is still a gap in the field concerning the impact behavior of sandwich panels with natural fiber faces such as FFRPs.

The existing modelling techniques for impact on composite sandwich panels typically assume that the face acts in a linear behaviour [17] as is typical for panels with synthetic FRP faces. However, numerous authors have shown that FFRPs exhibit a nonlinear stress-strain response under tensile [6, 8, 36–39] and compressive loads [8]. Additionally, it is known that foam materials behave in a nonlinear manner under shear loading [40]. Therefore, to more accurately model the behavior of sandwich panels with FFRP faces, the analysis must account for the nonlinear behavior of the face and foam materials. There are currently no models available for sandwich panels with FFRP faces with nonlinear mechanical behavior under impact loading in the literature.

This paper fills gaps in the field of study by providing test data on sustainable sandwich panels constructed with bio-based materials as well as presenting an accurate analytical procedure for predicting their behavior under impact loads. In this study, the effect of low velocity impact of a large

mass on one-way sandwich panels is investigated. The sandwich panels were constructed using foam cores and natural FFRP faces and were tested under a drop weight impact multiple times with increasing energy until ultimate failure. An analytical model has been developed to predict their behavior under these loading conditions. The model is based on the energy balance method and includes the effect of the nonlinear mechanical behavior of the FFRP faces and the foam core.

2. EXPERIMENTAL PROGRAM

2.1. Test Matrix

Nine sandwich panels were fabricated with foam cores and FFRP faces for drop weight impact tests. The main parameters of the study were the effect of facing thickness and core density on the impact behaviour of these panels. The test matrix is presented in Table 1. The naming convention is as follows: XFL-CYY, where X is the number of flax layers (1, 2 or 3) and YY is the nominal core density in kg/m^3 (32, 64 or 96). For example, a specimen with faces comprised of a one-ply FFRP and a foam core density of 96 kg/m^3 is referred to as 1FL-C96. The one, two and three layers of FFRP correspond to nominal face thicknesses of 1.5, 2.5 and 3.5 mm.

2.2. Materials

For the specimen cores, three different closed cell polyisocyanurate foams were used. The nominal core densities were 32 kg/m^3, 64 kg/m^3 and 96 kg/m^3 and were measured to be 31.2 kg/m^3, 62.4 kg/m^3 and 91.7 kg/m^3, respectively, by Codyre et al. [7]. The FFRP faces were fabricated with a balanced bidirectional flax fabric with a measured areal density of 410 g/m^2 and epoxy with a bio-content of 30% after mixing. The properties of these FFRPs were measured in a previous study by testing five identical two-ply bidirectional FFRP tensile tension coupons (average thickness of 3.0 mm) and five identical eight-ply bidirectional FFRP compression coupons (average thickness of 24 mm) [8]. The

measured tensile strength, the initial Young's modulus and the ultimate strain were 45.4 ± 1.8 MPa, 7.51 ± 0.69 GPa and 0.0083 ± 0.0009 mm/mm, respectively. The measured initial compressive Young's modulus was 6.73 ± 1.59 GPa and the compressive strength and corresponding strain were 86.4 ± 2.2 MPa and 0.0327 ± 0.0010 mm/mm, respectively.

2.3. Specimen Fabrication

The specimen fabrication process is shown in Figure 1. The foams were supplied in 1200 mm x 2400 mm sections and were cut down to a size of 1200 mm x 600 mm for fabrication. To fabricate the specimens, the top face of the foam was first cleaned of all debris and then coated with epoxy. A layer of dry fabric was placed on the face (with its warp direction parallel to the longitudinal direction of the specimens) and coated with epoxy. This procedure was repeated as required for each facing thickness. After placing the last layer of fabric and epoxy, a layer of parchment paper was applied to the face and all excess resin and air were removed using an aluminum roller. The specimen was then covered with a weighted flat board and allowed to cure for seven days, after which the other face was completed following the same procedure. Once both faces were completed, four identical 150 mm wide specimens were cut from the 600 mm wide section using a band saw.

2.4. Test Setup and Instrumentation

The drop-weight test set-up is presented in Figure 2. Strain gauges were installed at the centre of the top and bottom faces at mid-span. A fast-action string potentiometer was connected to the bottom face of the specimen and an accelerometer was attached to the drop weight. The data was sampled at a rate of 25 kHz. Additionally, a video of each test was recorded by a camera with a frame rate of 500 fps. The bottom of the drop weight impact was fitted with a 9.5 mm thick section of a steel hollow structural section (HSS) impact surface 150 mm wide as shown in Figure 2. This impact surface was used to limit the potential for local indentation. To avoid damaging the strain gauge on the top face,

a 25 mm diameter hole was cut into the center of the HSS impact surface. The mass of the drop weight was 10.413 kg. Each specimen was tested multiple times until failure starting at a drop height of 100 mm and increased by increments of 100 mm. This test procedure meant that each specimen was tested a different number of times depending on the maximum drop height that was resisted. Note that specimen 2FL-C64 was tested first and started at a height of 300 mm and incremented likewise. After testing this specimen, it was decided that this increment did not yield enough data and therefore the starting height and increment were decreased to the 100 mm used for the remaining specimens. For specimen 3FL-C96, the maximum possible drop height of the test frame (2100 mm) was achieved before ultimate failure. Therefore, the drop weight mass was increased by 6.015 kg and the tests were restarted at a height of 1395 mm, such that the energy was equivalent to the original mass dropped from a height of 2200 mm. It is recognized that, while the energy level increment was maintained, the impact velocity increment was affected by this procedure. However, as the maximum possible drop height was reached, this was the only available option to maintain the energy level increments for testing. The height increment was also reduced to 63 mm such that the increase in impact energy remained constant between tests.

3. EXPERIMENTAL RESULTS AND DISCUSSIONS

The main results obtained through these tests were the ultimate impact resistance (E), maximum deflection (Δ), and the maximum strain in each face (ϵ_t and ϵ_c). Note that for this discussion the ultimate energy resistance is the maximum impact energy at which specimen did not experience failure and the energy failure is the impact energy at which the specimen experienced ultimate failure. Additionally, the specimen stiffness (K) and damping ratio (ζ) were calculated based on the deflection measurements. The data in this study was processed using both Matlab and the scientific Python

package, Anaconda. Due to electrical noise in the deflection readings, the data was filtered using a moving average filter. Though this filter affected the amplitude of the measurements, upon inspection it was determined that the data remained accurate to within 0.1 mm (< 0.5%) after filtering. The strain gauge data was unaffected by this noise.

3.1. Energy Resistance and Failure Modes

Figure 3 presents a bar chart showing the maximum energy resisted by each panel type and compares the energies to those resisted by the panels tested under quasi-static load by Betts et al. [8]. There was a large variation in energy capacity between the different panels; the strongest panel (3FL-C96) resisted a maximum impact energy of 245 J before ultimate failure whereas the weakest panel (1FL-C32) resisted only 10.2 J. The figure shows that the capacity increased with core density. For instance, specimen 3FL-C32 resisted a maximum of energy of 91.9 J whereas specimen 3FL-C64 resisted a maximum energy of 173.7 J, an increase of 89%. Again, going from specimen 3FL-C64 to specimen 3FL-C96 there was an increase in capacity of 41%. Panel capacity also increased with facing thickness. Specimen 1FL-C96 resisted a maximum energy of 61.3 J whereas, increasing the face thickness by one layer of flax fabric, 2FL-C96 resisted an energy of 163.4 J, an increase of 167%. Similarly, increasing the facing thickness by one more layer of flax fabric yielded another increase in capacity of 41%.

The dynamic and static energies are similar for most specimens, however, specimens 2FL-C64 and 3FL-C64 exhibited less energy resistance under static loading. In the study by Betts et al. [8] it was noted that specimen 2FL-C64 was tested with two pinned supports which may have reduced its ultimate capacity. Also, upon examination of the test results of their study, the deflection of specimen 3FL-C64 was overpredicted by the model by 56% whereas the next highest overprediction was only

30%. This indicates that the static specimen potentially experienced premature failure and would therefore account for the difference between the static and dynamic capacities.

Figure 4 presents a comparison of the failure modes exhibited during the static and dynamic tests. It shows that all the specimens save one failed in the same manner in the static and dynamic tests. The exception is specimen 2FL-C64. However, as mentioned previously, this specimen was tested at drop height increments of 300 mm. Therefore, there is the potential that the impact causing failure was well above the actual ultimate capacity of the specimen and caused it to fail in a different manner than it would have had it been impacted by an energy closer to its actual capacity. The fact that the energy levels and failure modes are comparable between the static and dynamic tests indicates that there is the potential to use the failure mode maps presented by Betts et al [8] to predict the failure mode of these panels under impact loading. It also indicates that it may be viable to determine impact properties of similar foam-core FFRP sandwich panels using only quasi-static testing.

3.2. Specimen Deflections and Face Strains

Figure 5 shows the effect of face thickness on the maximum deflection. For specimens with higher core densities the deflection decreased with facing thickness. For example, at an energy level of 51.1 J, the deflection of specimen 1FL-C96 is 26.9 mm which is a 27% increase from the 21.1 mm deflection of 2FL-C96 and a 60% increase from the 16.8 mm deflection of specimen 3FL-C96. Interestingly, from Figure 5a (specimens with a core density of 32 kg/m^3), the face thickness has less influence on the deflection at each energy level than it did for the higher density foam-cored specimens. This is indicative that the shear deflection in specimens with weaker cores is more prominent than in specimens with higher density cores. This behavior is discussed further in the modelling section of this paper.

Figure 6 presents the effect of face thickness on the strain in each face at mid span. Note that compressive strain is represented as negative and tensile strain is represented as positive. Looking at Figure 6a, specimens 2FL-C32 and 3FL-C32 exhibit similar face strains whereas the face strains of specimen 1FL-C32 are greatly increased when compared to specimen 2FL-C32, especially on the bottom face. This indicates that the bending deflection is more prevalent in this specimen, whereas shear deflection may govern the deflection behaviour of the specimens with thicker faces. This trend is also evident to a lesser degree in Figures 6b and 6c. For all core types, face strain increased with a decrease in face thickness and the largest increase in face strain is observed when moving from a face with two layers of flax to a face with one layer of flax.

3.3. Calculation of Specimen Stiffness

The damped period of the structure was them determined based on the first natural frequency by calculating the average time between the peaks and troughs of the deflection data. The damped angular frequency could then be calculated by:

$$\omega_d = \frac{2\pi}{T_d} \tag{1}$$

where ω_d is the damped angular frequency and T_d is the damped period of the sandwich panel, the average values of which are presented in Table 2. The natural angular frequency and damping ratio could then be determined by:

$$\omega_n = \frac{\omega_d}{\sqrt{1-\xi^2}} \tag{2}$$

$$f(t) = Ce^{\xi\omega_n t} \tag{3}$$

where C is a constant, ξ is the damping ratio based on the first natural frequency, ω_n is the natural angular frequency, and t is time. Eq. 3 was fit to the peak values of the free vibration portion of

deflection versus time plot. An example of the fit of Eq. 3 is shown for specimen 2FL-C64 impacted using a drop height of 1200 mm in Figure 7c. The specimen stiffness was calculated by:

$$K = \frac{{\omega_n}^2 mL}{2} \quad (4)$$

where m is the specimen mass per unit length, and L is the span length. Figure 8 shows the effect of the facing thickness on the specimen stiffness. The stiffness does not change significantly after multiple tests of each specimen which supports the observation during the tests that there was no significant observable damage before ultimate failure. While it is possible that unobservable microscopic damage could be caused by an impact event, this would be evidenced by a reduction in specimen stiffness. Therefore, the test results do not support the presence of microscopic damage due to the repeated impact events throughout testing. This also means that the specimen stiffness can be taken as the average stiffness calculated from the data of each test, which is presented in Table 2. From Figure 8, it is evident that stiffness increased with facing thickness. For specimens with weak cores (32 kg/m^3), the effect of face thickness is less significant. This is because these specimens are more affected by shear deflection that the specimens with stronger cores. Table 2 shows there is a 54% increase in average stiffness from specimen 1FL-C96 to specimen 2FL-C96 and a 36% increase from specimen 2FL-C96 to specimen 3FL-C96. It is also evident that stiffness increased with core density. For example, specimen 2FL-C32 exhibited a stiffness of 94.8 N/mm, whereas specimen 2FL-C64 exhibited a stiffness of 133.0 N/mm, which is an increase of 40%. The stiffness of specimen 2FL-C96 was found to be 192.1 N/mm, an increase of 44% from specimen 2FL-C64.

4. ANALYTICAL STUDY

As a part of this study, a nonlinear incremental iterative model (NIIM) was developed to predict deflection and face strain during an impact event based on the conservation of energy. The NIIM

assumes that the potential energy of the drop is completely absorbed by the shear and flexural bending induced in the sandwich panel due to the impact. This section presents the development and the verification of the deflection and face strain models.

4.1.Nonlinear Behavior of Constituents

As found by numerous authors, FFRPs typically exhibit nonlinear mechanical behavior [6, 8, 36–39]. It is also known that core foams typically exhibit a nonlinear shear stress-strain response [40]. Therefore, to accurately predict the behavior of sandwich panels with FFRP faces and foam cores, it is important to consider the nonlinearity of the constituent materials.

Behavior of FFRP Faces

The behavior of the FFRP faces was modelled using a parabolic equation, presented in Eq. 5. Previously, the authors used a simple bi-linear model to predict the behavior of FFRP faces for sandwich panels tested under static loading [8]. However, this bi-linear model was intended to simplify the analysis for use in a design-oriented model. To improve the NIIM accuracy a parabolic model was chosen for the current study. The parabolic model was developed based on the assumptions that the initial slope was E_{fo}, the initial FFRP modulus determined through testing, and the ultimate stress-strain point was defined by σ_{fu}, the ultimate FFRP stress and ϵ_{fu}, the ultimate FFRP strain, both determined through testing.

$$\epsilon_f = \frac{\sigma_f^2}{\sigma_{fu}^2}\left(\epsilon_{fu} - \frac{\sigma_{fu}}{E_{fo}}\right) + \frac{\sigma_f}{E_{fo}} \tag{5}$$

Behavior of Foam Cores

To model the shear stress-strain behavior of the cores, a cubic model was developed and is presented in Eq. 6. A model verification using data from an independent study [41] is shown in Figure 10a and

the results and the shear stress-strain behavior of the core foams used in the current study are shown in Figure 10b.

$$\tau_c = \frac{2}{\gamma_{cu}^3}[0.55G_{co}\gamma_{cu} - \tau_{cu}]\gamma_c^3 + \frac{1}{\gamma_{cu}^2}[3\tau_{cu} - 2.1G_{co}\gamma_{cu}]\gamma_c^2 + G_{co}\gamma_c \quad (6)$$

where τ_c is the shear stress in the core, γ_c is the shear strain in the core, τ_{cu} is the ultimate core shear stress, γ_{cu} is the ultimate core shear strain and G_{co} is the initial modulus of the core. The equation was developed based on the following four boundary conditions: $\{\gamma_c = 0;\ \tau_c = 0\}$, $\{\gamma_c = \gamma_{cu};\ \tau_c = \tau_{cu}\}$, $\{\gamma_c = 0;\ d\tau_c/d\gamma_c = G_{co}\}$ and $\{\gamma_c = \gamma_{cu};\ d\tau_c/d\gamma_c = G_{co}/10\}$.

Modelling of Constituent Behavior Using a Secant Moduli

To incorporate the nonlinear behavior of the FFRP faces and foam core in the NIIM, a secant elastic modulus and a secant shear modulus were used at each energy level. This allowed the process to be incremented assuming a linear elastic behavior at each increment while also capturing the overall nonlinear behavior. The method of determining the secant moduli is shown in Figure 11. Each secant modulus was defined between a stress-strain of zero and a stress-strain point corresponding to the energy level. At each model increment an iterative procedure was used to determine the secant moduli to within an accuracy of 0.1%. The entire NIIM is presented in the form of a flowchart in Figure 12 and is detailed in the proceeding section.

4.2. Model Description

The NIIM presented in this section is an nonlinear analysis based on the energy balance method presented by Akil Hazizan and Cantwell [17] at multiple increments. At each model increment, the governing equation is as follows:

$$E_T = mgh = E_b + E_s + E_c \quad (7)$$

where E_T is total energy, m is the mass of the drop weight in kg, h is the drop height in m and E_b, E_s and E_c are the energies absorbed through bending, shear and contact, respectively. Eq. 7 assumes no loss of energy during the drop. Additionally, a steel section cut from a 150-mm wide Hollow Structural Section (HSS) was used as the impact surface to eliminate localized effects such as indentation. An HSS was chosen for its curved edges to eliminate the possibility of a stress concentration at the edge of the loading area. Additionally, the length of the impact surface was longer than the width of the specimens which ensured the entire width of each specimen was loaded. No indentation was observed during or after testing the sandwich specimens. Therefore, the model was developed with the assumption that the impact did not cause significant indentation in the top face sheet (i.e. the contact energy $E_c = 0$). Allen [2] presented a general load-displacement relationship for one-way sandwich panels subjected to three-point bending as shown in Eq. 8:

$$\delta = \frac{PL^3}{48D} + \frac{PL}{4AG} \tag{8}$$

where δ is the deflection, P is the equivalent static load, L is the span length, G is the secant shear modulus, $A=Gbd^2/c$ is a geometric property [2], b is the specimen width, t is the thickness of the faces, c is the thickness of the core and D is the flexural rigidity of the sandwich panel as follows:

$$D = \frac{1}{6}E_f bt^3 + \frac{1}{12}E_c bc^3 + \frac{1}{2}E_f btd^2 \tag{9}$$

where E_f is the secant modulus of elasticity of the FFRP faces. By using a variable secant modulus for the FFRP faces and foam cores, each model step can be analysed assuming linear-elastic behavior, while capturing the overall nonlinear behavior of the structure. Therefore, the total energy at each model increment must be equal to $E_t=P\delta_{max}/2$ and by rearranging with Eq. 7 and 8, the maximum impact force at each increment can be written as follows:

$$P_{max} = \sqrt{\frac{2mgh}{\frac{L^3}{48D} + \frac{L}{4AG}}} \quad (10)$$

The maximum impact force can then be used to predict the maximum strain experienced by each face during the test. To simplify this calculation, it is assumed that the neutral axis of the specimens is adequately close to the center of the cross section, such that the facing strain in the top face is equal and opposite to that in the bottom face. This assumption was used and verified by Betts et al. [8]. The first step in converting the impact force to face strain is to determine the moment due to the impact force. As it is a three-point bending configuration, this can be determined using by $M = P_{max}L/4$. The stress in each face can then be calculated by $\sigma_f = M/tdb$ and converted to strain in each face by dividing by the secant modulus of elasticity.

4.3. Model Verification

A comparison between the test data and the model at a selected energy level for each specimen is presented in Table 3. The table shows that, generally, the NIIM was able to accurately predict both the maximum deflection and face strain at each impact level. At the selected energy levels, the Test/NIIM ratios were 0.91 and 1.12 for midspan deflection and face strains, respectively.

Figure 13 and Table 3 show the verification of the deflection model. The test data presented in Figure 13 is the maximum deflection recorded from each impact event. The models presented do not predict ultimate energies, only the deflection behavior of the specimens. Each model was truncated at the ultimate failure energy recorded for the corresponding specimen. Note that some deflection data is missing due to instrumentation failure during the tests.

The model predicts the deflections of most specimens well, however, it over predicts deflection for all the specimens with the C96 foam cores. One hypothesis for this over prediction is that the mechanical properties of this foam are more affected by strain rate than the lower density foams. This would cause the specimen to be stiffer, reducing the overall deflection during the tests. Because specimens 2FL-C96 and 3FL-C96 reached higher energies (i.e. higher drop heights and higher strain rates) than the other specimens, this increase in stiffness could also be affected by the high strain rate behavior of the FFRP faces not seen in lower energy tests. Generally, as natural fibers are more variable than synthetic fibers all the results could be affected by the intrinsic variability of the natural flax fiber fabrics used. Additionally, the test data may vary because the specimens were impacted multiple times which could have caused unobservable microscopic damage. However, as discussed previously, the presence of microscopic damage is not supported by the test results.

Unlike most structures, shear deformation can significantly contribute to the overall deflection of sandwich structures. Therefore, it is important to consider the effect of the test parameters on shear deformation. Figure 14 shows the average contribution of both shear and bending to the overall deflection calculated by the model. This was calculated by separating the amount of shear and bending deflection calculated by Eq. 8. This figure shows that as the core strength increases the contribution of shear deflection on the overall specimen deflection decreases. It also shows that the most significant increase in shear deflection occurs when the core density is decreased from 64 kg/m^3 to 32 kg/m^3. For instance, the average percentage of shear contribution to the overall deflection of specimen 2FL-C32 is 82% whereas the average shear contributions to the deflections of 2FL-C64 and 2FL-C96 are 61% and 55%, respectively. This information suggests that in the design of sandwich structures with FFRP faces where the deflection criteria is important, the choice of core density is significant. Figure 14 also shows that the face thickness affects the contribution of shear and bending to the overall specimen

deflection. For all core types, as the face thickness increases, the contribution of shear deflection increases. However, this increase in contribution is due to the increase in flexural rigidity and not due to a significant increase in shear deflection.

Figure 15 and Table 3 show the verification of the strain model. It is important to note that this model does not predict the ultimate impact energy. Also note that some data points are missing due to failure of strain gauges in some of the tests. Generally, Figure 15 shows that the NIIM can reasonably predict the maximum strain in each face during the impact event.

One limitation of the NIIM is the assumption that the neutral axis is at the midsection. The accuracy of the model, specifically for predicting face strains, could be improved by determining the actual location of the neutral axis and considering the difference in tension and compression behavior of the faces. Future research will include experimental and analytical tests of the residual strength of these sandwich panels after an impact event.

5. CONCLUSIONS

In this paper, the results of drop weight impact tests on nine sandwich panels with flax fiber-reinforced polymer facings were discussed. The main parameters of the tests were the facing thickness (1, 2 or 3 layers of a balanced bidirectional flax fabric) and core density (32 kg/m^3, 64 kg/m^3 or 96 kg/m^3). A Nonlinear Incremental Iterative Model (NIIM) based on the energy balance method was used to accurately predict the deflection and face strain based on the impact energy. The NIIM was also shown to predict well the contribution of shear and bending to the overall deflection of each specimen due to an impact load. Based on the test results and the model predictions the following conclusions were made:

- The impact resistance of the foam core FFRP sandwich panels increases with both facing thickness and core density. For example, by increasing the face thickness by one layer, 2FL-C64

was able to resist a 122.6 J impact whereas 1FL-C64 resisted only 30.6 J. Likewise, by increasing the core density, 2FL-C96 was able to resist 163.4 J of energy, an increase of 40.8 J when compared to 2FL-C64.

- As shown in Figure 3, failure energies and failure modes under impact closely matched those observed during quasi-static testing on counterpart specimens. This is also true of specimen stiffness, the average Impact/Static stiffness ratio being 1.07.
- As shown in Figure 8, panel stiffness was not significantly affected after multiple impacts and increased with both facing thickness and core density.
- The contribution of shear deflection decreased with an increase in core density and was most affected when core density was reduced from 64 kg/m^3 to 32 kg/m^3. This indicates that in designs where the deflection is a limiting factor the choice of core density is important.
- The nonlinear model was able to accurately predict the experimental behavior. The average Test/NIIM ratios at the selected energy levels were 0.91 and 1.12 for the specimen deflection and face strains, respectively.

6. ACKNOWLEDGEMENTS

The authors would like to thank Brandon Fillmore, Koosha Khorramian, Jesse Keane and Brian Kennedy for their assistance in the lab. The authors would also like to acknowledge and thank Bioindustrial Innovation Canada (BIC), Queen's University, and Dalhousie University for their in kind and financial support.

7. DATA AVAILABILITY

The raw/processed data required to reproduce these findings cannot be shared at this time due to

technical or time limitations.

8. REFERENCES

[1] Ramesh M, Palanikumar K, Reddy KH. Plant fibre based bio-composites : Sustainable and renewable green materials. *Renew Sustain Energy Rev* 2017; 79: 558–584.

[2] Allen HG. *Analysis and Structural Design of Sandwich Panels*. Oxford, UK: Pergamon Press, 1969.

[3] Cicala G, Cristaldi G, Recca G, et al. Composites Based on Natural Fibre Fabrics. In: Dubrovski PD (ed) *Woven Fabric Engineering*. IntechOpen, 2010. Epub ahead of print 2010. DOI: 10.5772/10465.

[4] Fam A, Sharaf T, Sadeghian P. Fiber element model of sandwich panels with soft cores and composite skins in bending considering large shear deformations and localized skin wrinkling. *J Eng Mech* 2016; 142: 1–14.

[5] Sadeghian P, Hristozov D, Wroblewski L. Experimental and analytical behavior of sandwich composite beams: Comparison of natural and synthetic materials. *J Sandw Struct Mater* 2018; 20: 287–307.

[6] Mak K, Fam A, Macdougall C. Flexural Behavior of Sandwich Panels with Bio-FRP Skins Made of Flax Fibers and Epoxidized Pine-Oil Resin. *J Compos Constr* 2015; 19: 1–13.

[7] CoDyre L, Mak K, Fam A. Flexural and axial behaviour of sandwich panels with bio-based flax fibre-reinforced polymer skins and various foam core densities. *J Sandw Struct Mater* 2018; 20: 595–616.

[8] Betts D, Sadeghian P, Fam A. Experimental Behavior and Design-Oriented Analysis of Sandwich Beams with Bio-Based Composite Facings and Foam Cores. *J Compos Constr*

2018; 22: 1–12.

[9] Tuo H, Lu Z, Ma X, et al. An experimental and numerical investigation on low-velocity impact damage and compression-after-impact behavior of composite laminates. *Compos Part B* 2019; 167: 329–341.

[10] Xiao L, Wang G, Qiu S, et al. Exploration of energy absorption and viscoelastic behavior of CFRPs subjected to low velocity impact. *Compos Part B* 2019; 165: 247–254.

[11] Zhang J, Pan S, Chen L. Dynamic thermal buckling and postbuckling of clamped–clamped imperfect functionally graded annular plates. *Nonlinear Dyn* 2019; 95: 565–577.

[12] Abrate S. Localized Impact on Sandwich Structures With Laminated Facings. *Appl Mech Rev* 1997; 50: 69.

[13] Anderson T, Madenci E. Experimental investigation of low-velocity impact characteristics of sandwich composites. *Compos Struct* 2000; 50: 239–247.

[14] Atas C, Potoglu U. The Effect of Face-Sheet Thickness on Low-Velocity Impact Response of Sandwich Composites with Foam Cores. *J Sandw Struct Mater* 2016; 18: 215–228.

[15] Schubel PM, Luo J-J, Daniel IM. Low velocity impact behavior of composite sandwich panels. *Compos Part A Appl Sci Manuf* 2005; 36: 1389–1396.

[16] Torre L, Kenny JM. Impact testing and simulation of composite sandwich structures for civil transportation. *Compos Struct* 2000; 50: 257–267.

[17] Akil Hazizan M, Cantwell WJ. The low velocity impact response of foam-based sandwich structures. *Compos Part B Eng* 2002; 33: 193–204.

[18] Plagianakos TS, Lika K, Papadopoulos EG. Low-velocity impact response of smart sandwich composite plates with piezoelectric transducers : Modeling and experiments. *J Intell Mater Syst Struct* 2016; 27: 774–785.

[19] Abrate S. *Impact on Composite Structures*. Cambridge, UK: Cambridge University Press, 1998.

[20] Icardi U, Ferrero L. Impact analysis of sandwich composites based on a refined plate element with strain energy updating. *Compos Struct* 2009; 89: 35–51.

[21] Malekzadeh K, Khalili MR, Olsson R, et al. Higher-order dynamic response of composite sandwich panels with flexible core under simultaneous low-velocity impacts of multiple small masses. *Int J Solids Struct* 2006; 43: 6667–6687.

[22] Christoforou AP, Yigit AS. Scaling of low-velocity impact response in composite structures. *Compos Struct* 2009; 91: 358–365.

[23] Andrews EW, Moussa NA. Failure mode maps for composite sandwich panels subjected to air blast loading. *Int J Impact Eng* 2009; 36: 418–425.

[24] Zhu S, Chai GB. Damage and failure mode maps of composite sandwich panel subjected to quasi-static indentation and low velocity impact. *Compos Struct* 2013; 101: 204–214.

[25] Kalantari M, Nami MR, Kadivar MH. Optimization of composite sandwich panel against impact using genetic algorithm. *Int J Impact Eng* 2010; 37: 599–604.

[26] De Cicco D, Taheri F. Robust numerical approaches for simulating the buckling response of 3D fiber-metal laminates under axial impact – Validation with experimental results. *J Sandw Struct Mater*. Epub ahead of print 2018. DOI: 10.1177/1099636218789614.

[27] Zhou J, Hassan MZ, Guan Z, et al. The low velocity impact response of foam-based sandwich panels. *Compos Sci Technol* 2012; 72: 1781–1790.

[28] De Cicco D, Taheri F. Delamination Buckling and Crack Propagation Simulations in Fiber-Metal Laminates Using xFEM and Cohesive Elements. *Appl Sci* 2018; 8: 2440.

[29] Feng D, Aymerich F. Damage prediction in composite sandwich panels subjected to low-

velocity impact. *Compos Part A Appl Sci Manuf* 2013; 52: 12–22.

[30] Besant T, Davies GAO, Hitchings D. Finite element modelling of low velocity impact of composite sandwich panels. *Compos - Part A Appl Sci Manuf* 2001; 32: 1189–1196.

[31] Nguyen MQ, Jacombs SS, Thomson RS, et al. Simulation of impact on sandwich structures. *Compos Struct* 2005; 67: 217–227.

[32] Meo M, Vignjevic R, Marengo G. The response of honeycomb sandwich panels under low-velocity impact loading. *Int J Mech Sci* 2005; 47: 1301–1325.

[33] Zhang D, Jiang D, Fei Q, et al. Experimental and numerical investigation on indentation and energy absorption of a honeycomb sandwich panel under low-velocity impact. *Finite Elem Anal Des* 2016; 117–118: 21–30.

[34] Ude AU, Arif AK, Azhari CH. Impact damage characteristics in reinforced woven natural silk / epoxy composite face-sheet and sandwich foam, coremat and honeycomb materials. *Int J Impact Eng* 2013; 58: 31–38.

[35] Boria S, Raponi E, Sarasini F, et al. Green sandwich structures under impact: experimental vs numerical analysis. *Procedia Struct Integr* 2018; 12: 317–329.

[36] Hristozov D, Wroblewski L, Sadeghian P. Long-term tensile properties of natural fibre-reinforced polymer composites: Comparison of flax and glass fibres. *Compos Part B Eng* 2016; 95: 82–95.

[37] Christian SJ, Billington SL. Mechanical response of PHB- and cellulose acetate natural fiber-reinforced composites for construction applications. *Compos Part B* 2011; 42: 1920–1928.

[38] Mathura N, Cree D. Characterization and mechanical property of Trinidad coir fibers. *J Appl Polym Sci* 2016; 133: 1–9.

[39] Yan L, Kasal B, Huang L. A review of recent research on the use of cellulosic fibres, their

fibre fabric reinforced cementitious, geo-polymer and polymer composites in civil engineering. *Compos Part B Eng* 2016; 92: 94–132.

[40] Fam A, Sharaf T. Flexural performance of sandwich panels comprising polyurethane core and GFRP skins and ribs of various configurations. *Compos Struct* 2010; 92: 2927–2935.

[41] Sharaf T, Fam a. Numerical modelling of sandwich panels with soft core and different rib configurations. *J Reinf Plast Compos* 2012; 31: 771–784.

Table 1. Test matrix

No.	Specimen I.D.	Number of FFRP layers in each facing	Nominal core density (kg/m^3)	Number of Impacts
1	1FL-C32	1	32	2
2	2FL-C32	2	32	4
3	3FL-C32	3	32	7
4	1FL-C64	1	64	4
5	2FL-C64	2	64	5 *
6	3FL-C64	3	64	17
7	1FL-C96	1	96	10
8	2FL-C96	2	96	18
9	3FL-C96	3	96	25

* *This specimen was tested at drop height increments of 300 mm*

Table 2. Summary of impact test results and comparison with static tests

Specimen I.D.	Impact Energy Resisted (J)	Specific Absorbed Energy (J/kg)	Damped Period (s)		Impact Test Stiffness (N/mm)		Static Test Stiffness (N/mm)	Ratio of Impact to Static Stiffness
			AVE	SD	AVE	SD		
1FL-C32	10.2	10.4	0.0175	N/A	63.2	N/A	54	1.17
2FL-C32	30.6	20.0	0.018	0.0003	94.8	3.1	73.4	1.29
3FL-C32	91.9	46.0	0.0196	0.0012	97.5	10.6	87.7	1.11
1FL-C64	30.6	19.6	0.019	0.0001	84.2	0.7	100.8	0.84
2FL-C64	122.6	60.6	0.0173	0.0004	133.0	6.6	114.5	1.16
3FL-C64	173.7	69.7	0.0167	0.0006	172.4	11.4	161.1	1.07
1FL-C96	61.3	31.6	0.0174	0.0003	124.7	4.7	121.3	1.03
2FL-C96	163.4	66.3	0.0159	0.0006	192.1	14.7	206.5	0.93
3FL-C96	245.1	84.5	0.0147	0.0012	261.3	33.2	248.8	1.05
AVE								1.07
SD								0.14

Note: AVE = average and SD = standard deviation.

Table 3. Comparison of the Test Data and Results of the NIIM

		Deflection (mm)			Bottom Strain (mm/mm)			Top Strain (mm/mm)		
Specimen	Energy (J)	Test	NIIM	Test/NIIM	Test	NIIM	Test/NIIM	Test	NIIM	Test/NIIM
1FL-C32	10.2	19.0	18.9	1.01	0.0034	0.0020	1.70	-0.0003	-0.0020	0.15
2FL-C32	10.2	16.0	17.2	0.93	0.0015	0.0012	1.25	-0.0010	-0.0012	0.83
3FL-C32	10.2	16.3	17.0	0.96	0.0017	0.0010	1.70	-0.0010	-0.0010	1.00
1FL-C64	30.6	26.3	24.0	1.10	0.0071	0.0048	1.48	-0.0046	-0.0048	0.96
2FL-C64	30.6	20.3	21.0	0.97	0.0046	0.0032	1.44	-0.0026	-0.0032	0.81
3FL-C64*	30.6	16.3	19.5	0.84	0.0037	0.0031	1.19	-0.0026	-0.0031	0.84
1FL-C96†	61.3	29.8	32.9	0.91	0.0091	0.0067	1.36	-0.0071	-0.0067	1.06
2FL-C96	61.3	23.0	28.0	0.82	0.0067	0.0048	1.40	-0.0036	-0.0048	0.75
3FL-C96	61.3	18.2	26.4	0.69	0.0055	0.004	1.38	-0.0034	-0.0040	0.85
AVE				0.91			1.43			0.81
SD				0.12			0.18			0.27

* *Strain data and model compared at energy level of 51.1 J as strain gauge failed during 30.3 J impact test*

† *Strain data and model compared at energy level of 51.1 J as strain gauge failed during 61.3 J impact test*

Figure 1. Specimen fabrication: (a) mixing epoxy and section of cleaned foam; (b) application of epoxy; (c) specimen curing with weighted board; and (d) finished specimens

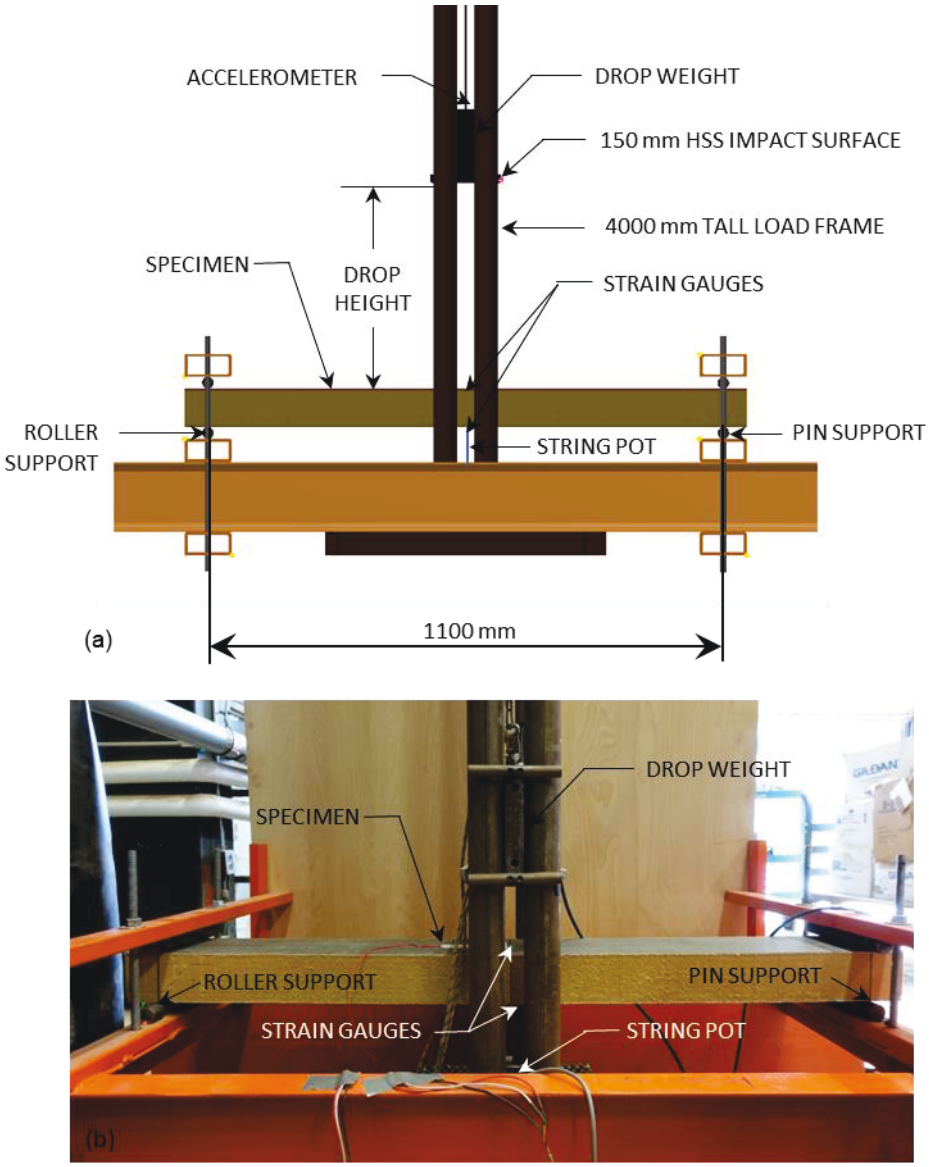

Figure 2. Test set-up: (a) schematic and (b) photo

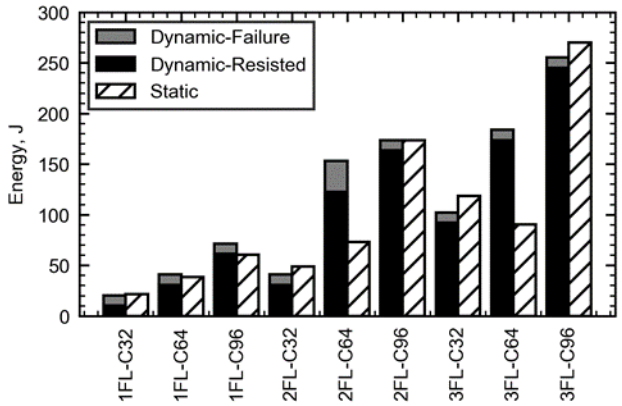

Figure 3. Comparison of energy resistance between dynamic and static tests

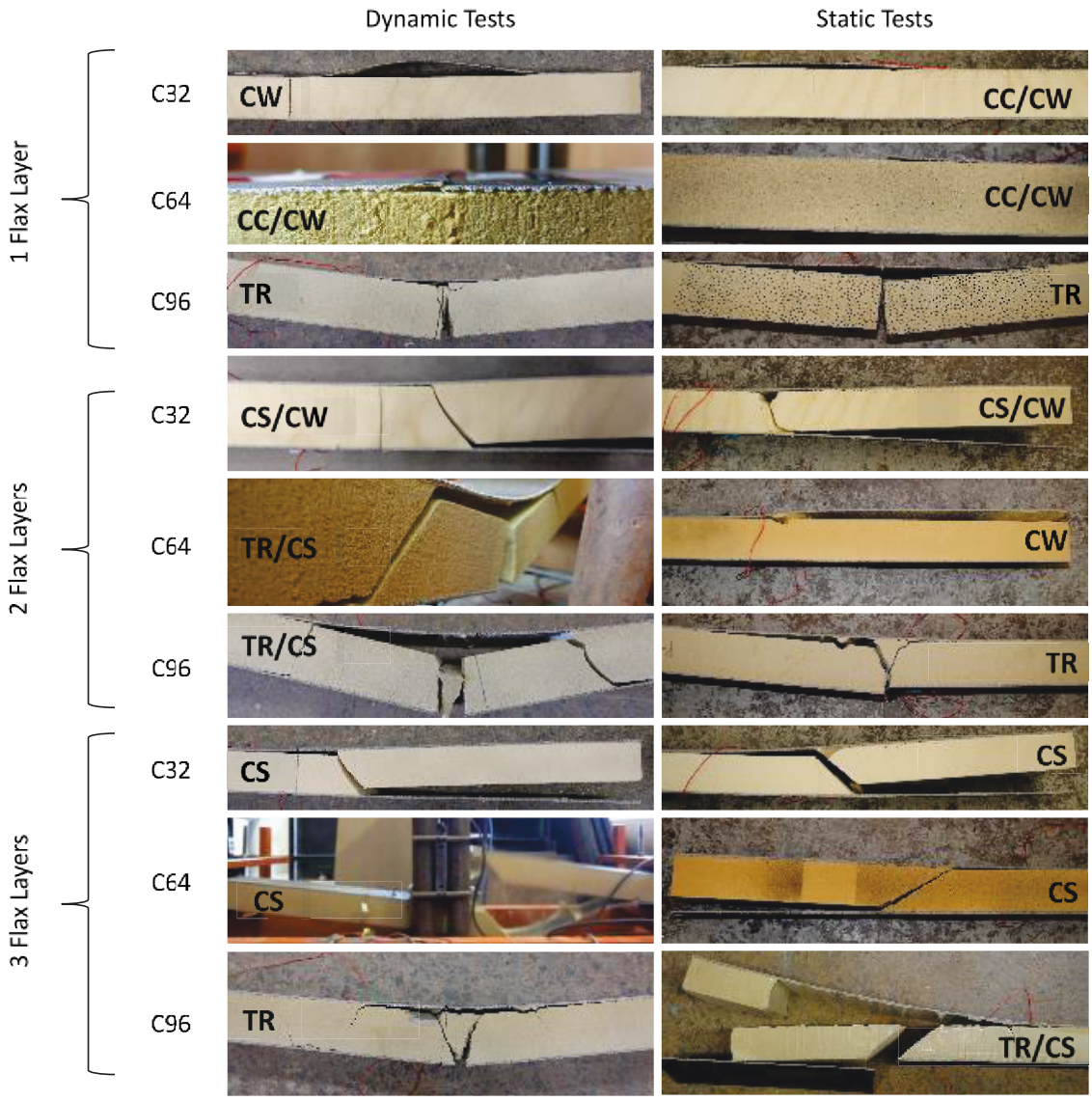

Figure 4. Comparison of static and dynamic failure modes (Note: CC = Compression Crushing; CW = Compression Wrinkling; CS = Core Shear; and TR = Tensile Rupture)

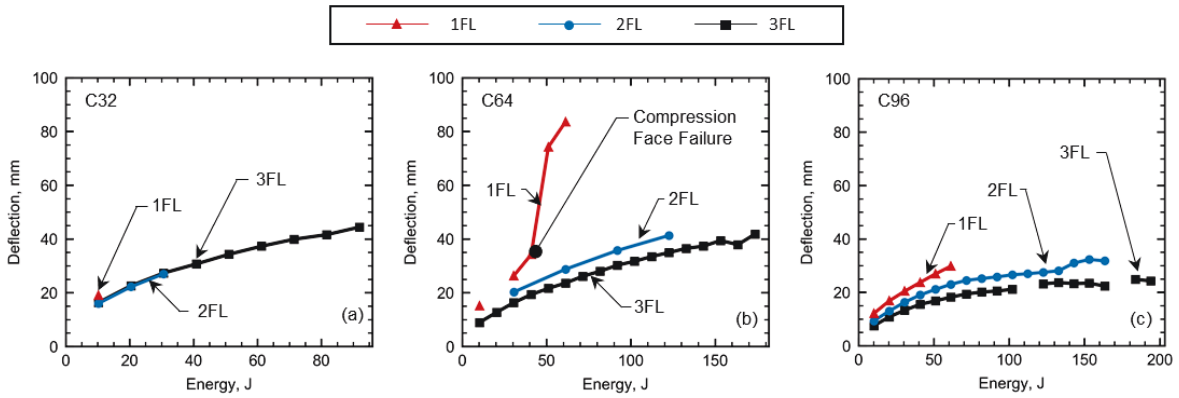

Figure 5. Measured maximum deflection at mid-span during each impact event: (a) C32; (b) C64; and (c) C96

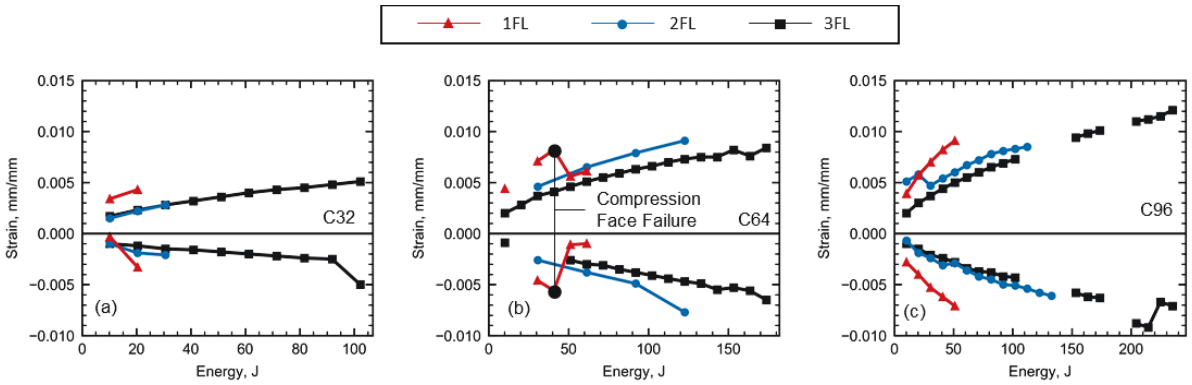

17

18 **Figure 6. Measured maximum face strains at midspan during each impact event: (a) C32; (b)**

19 **C64; and (c) C96 (Note: top face strains are negative; bottom face strains are positive)**

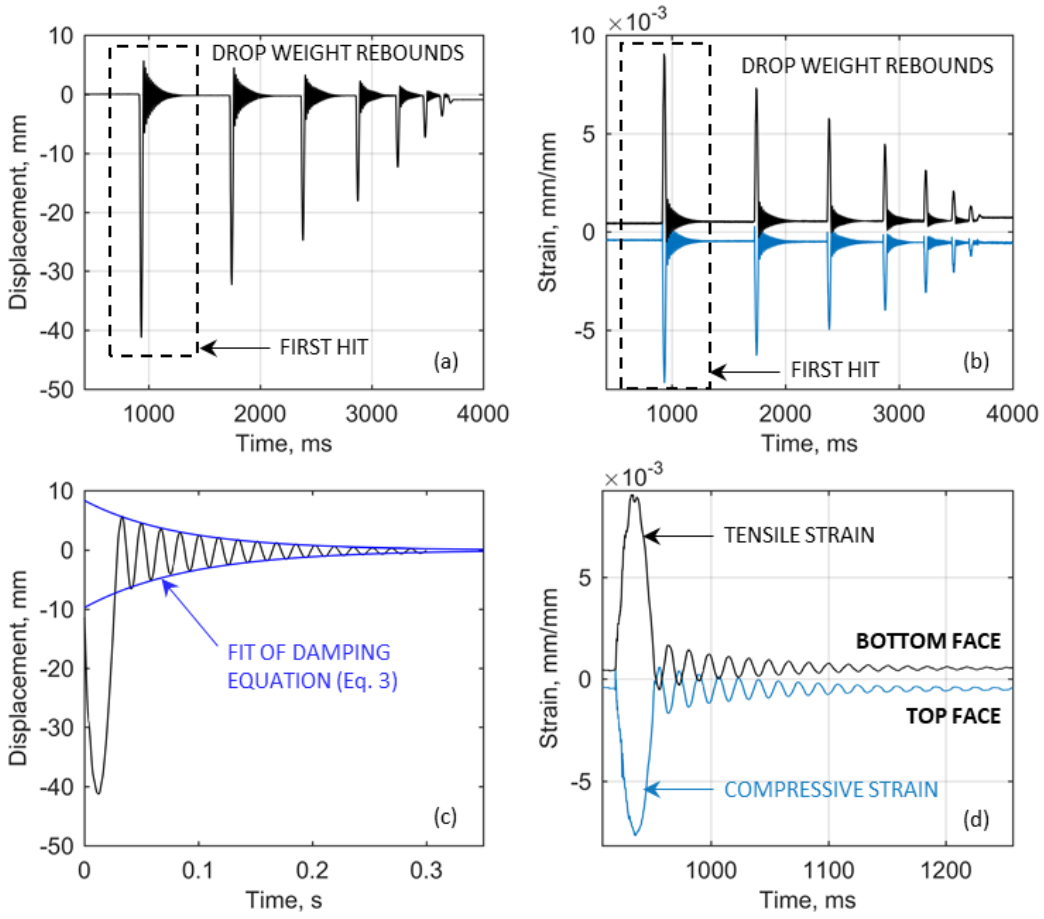

Figure 7. Measured data for a drop height of 1200 mm on specimen 2FL-C64: (a) midspan displacement during test; (b) midspan face strain during test; (c) displacement due to first hit; and (d) face strains due to first hit

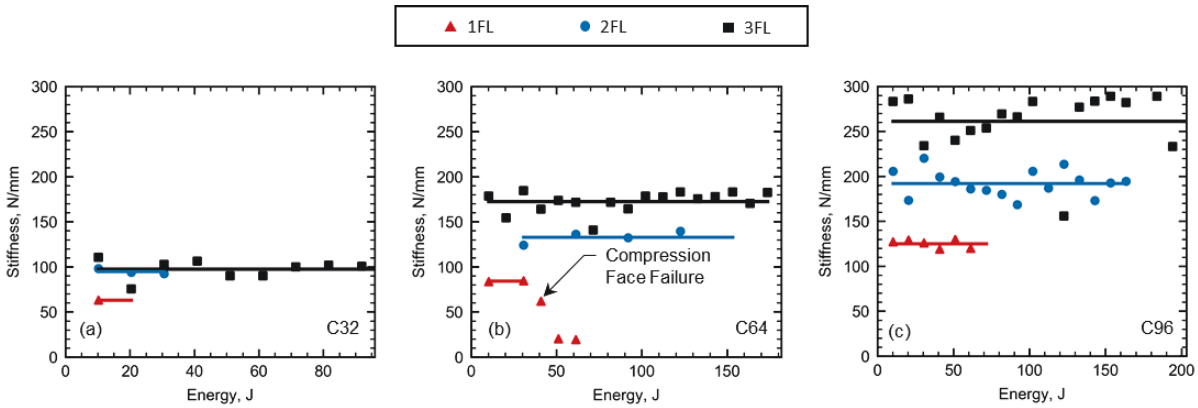

Figure 8. Calculated stiffness during each impact event: (a) C32; (b) C64; and (c) C96 (Note: lines represent the average calculated stiffness)

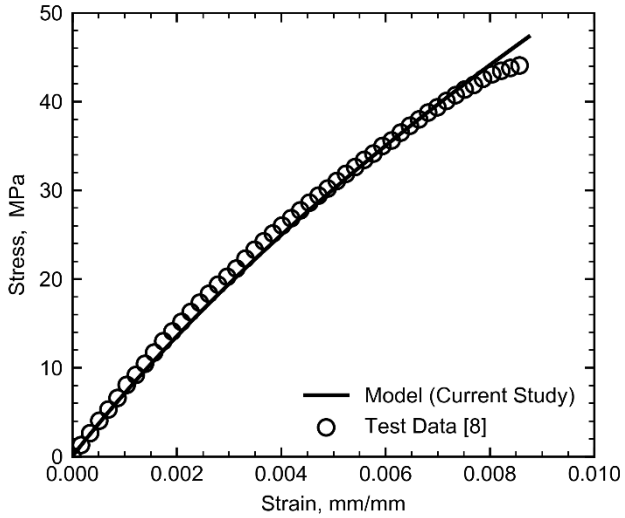

29

30 **Figure 9: Verification of FFRP face parabolic model against test data from an independent**

31 **study**

32

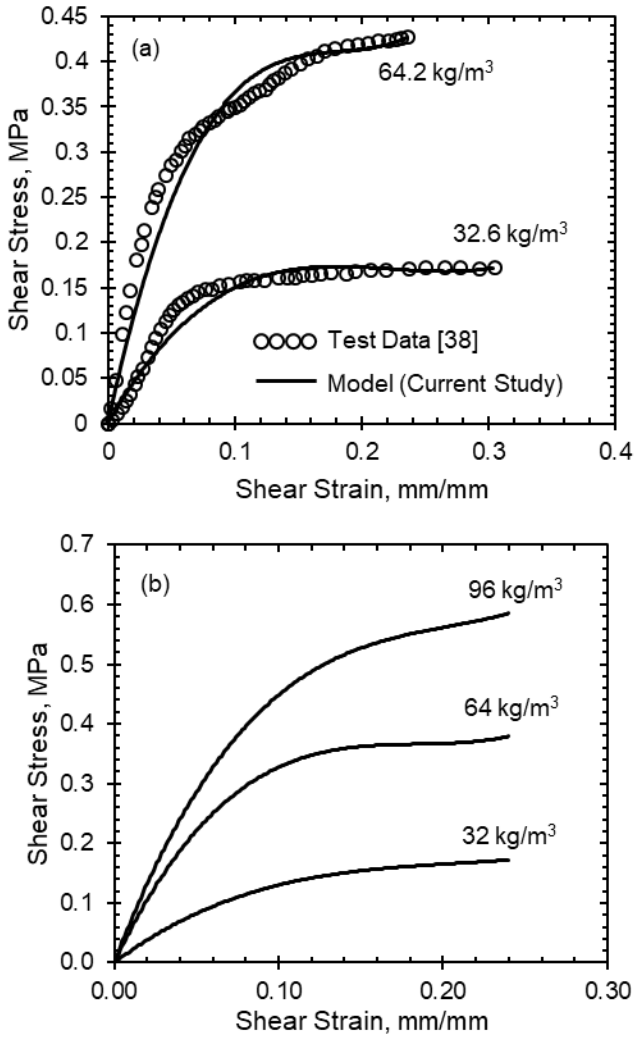

33

34 **Figure 10: Modelling of shear stress-strain response of foam cores (a) verification using**

35 **independent data and (b) models used in the current study**

36

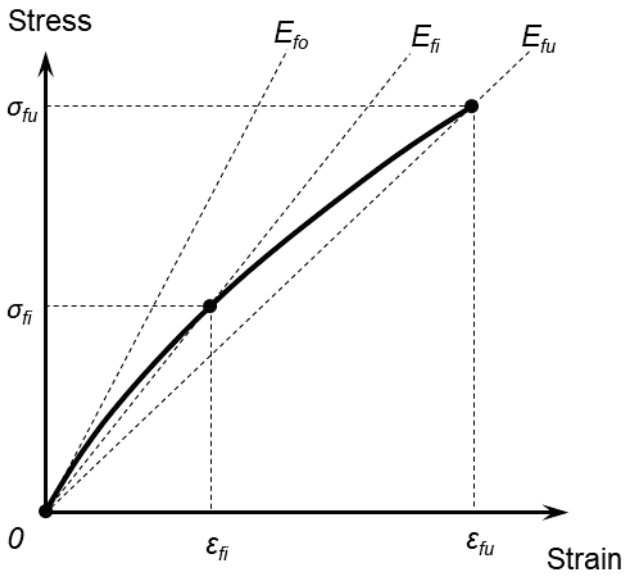

Figure 11. Modelling of nonlinear mechanical behavior using variable secant moduli

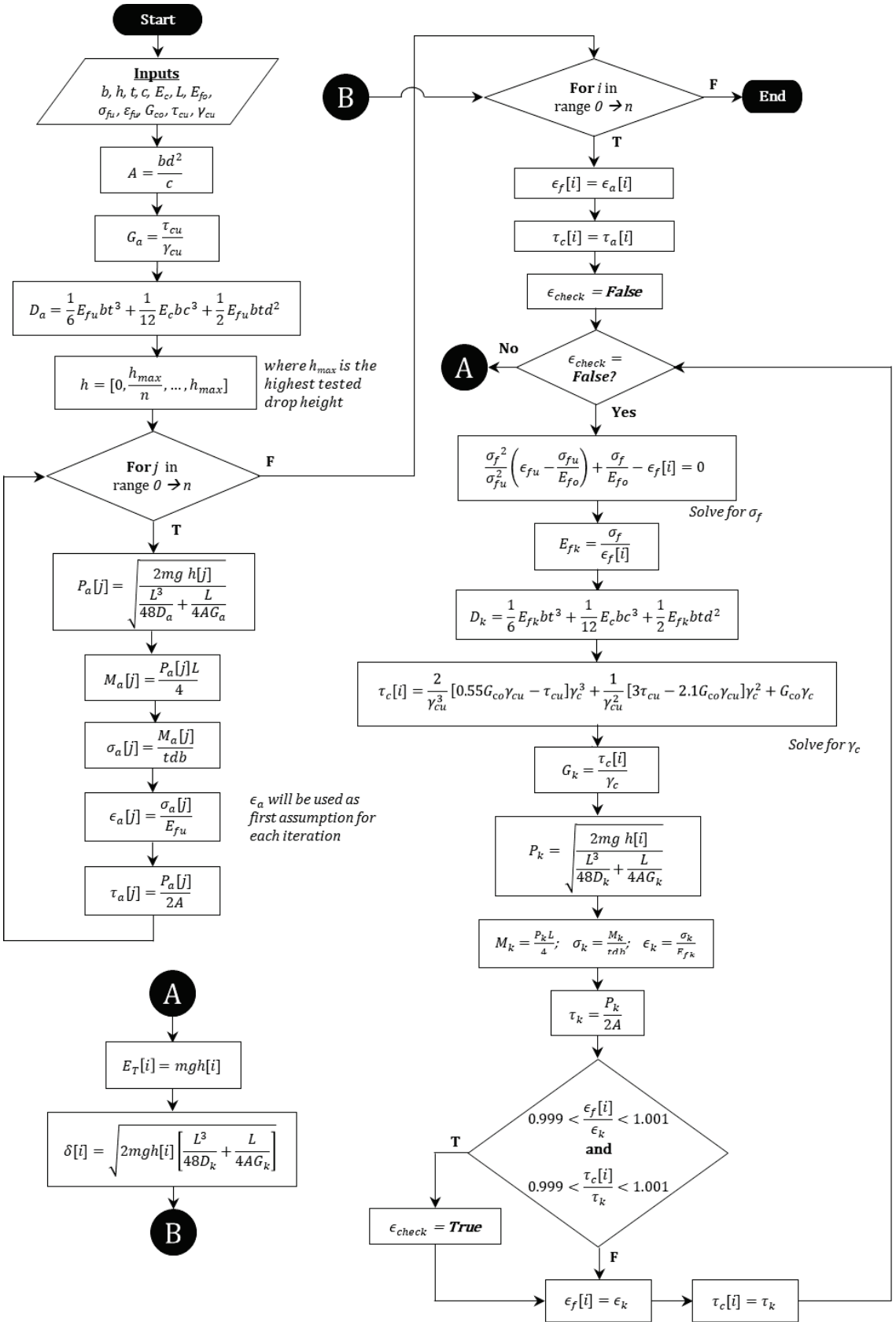

Figure 12. Analysis flow chart

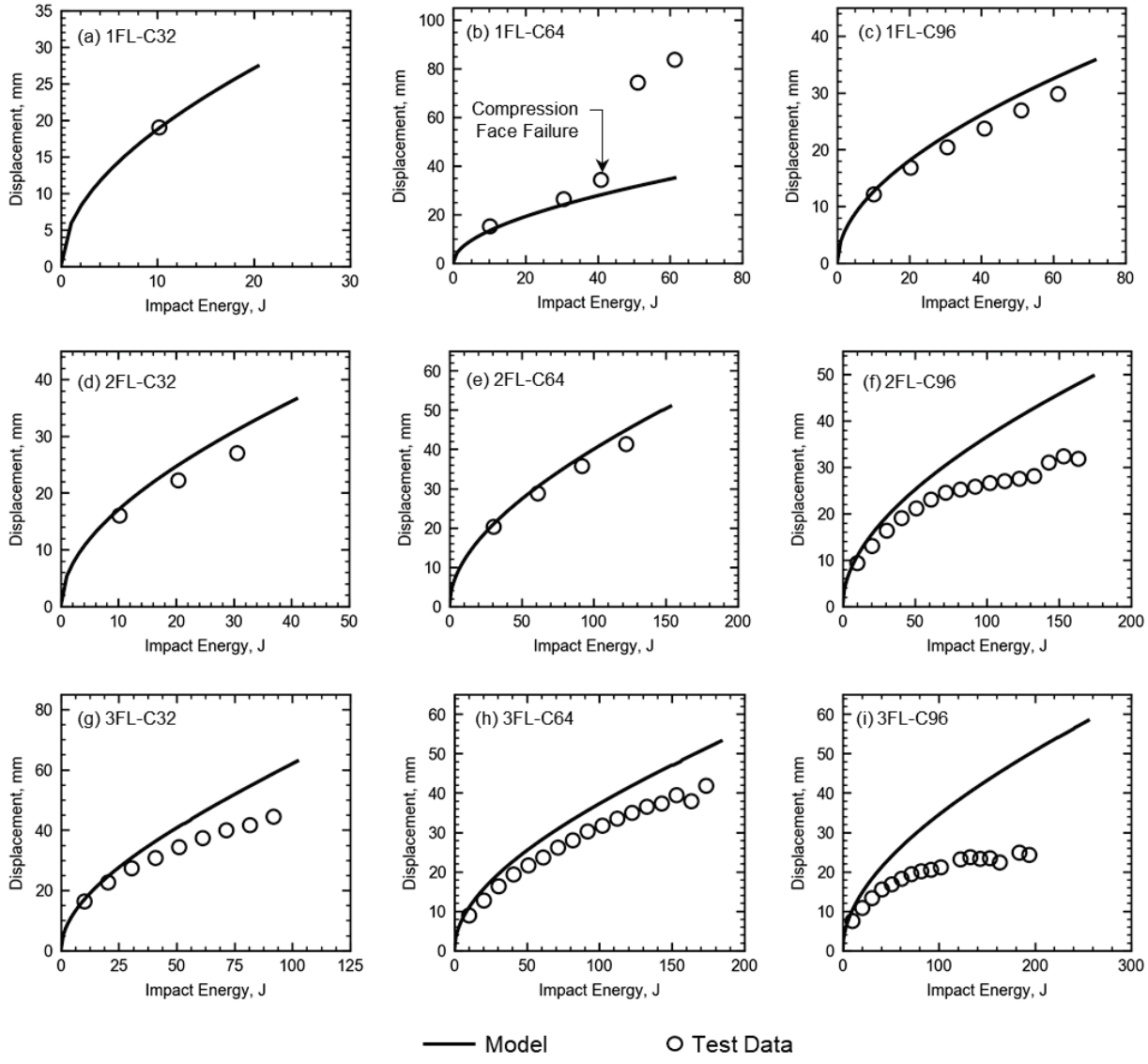

Figure 13. Verification of deflection model against test data: (a) 1FL-C32; (b) 1FL-C64; (c) 1FL-C96; (d) 2FL-C32; (e) 2FL-C64; (f) 2FL-C96; (g) 3FL-C32; (h) 3FL-C64; and (i) 3FL-C96

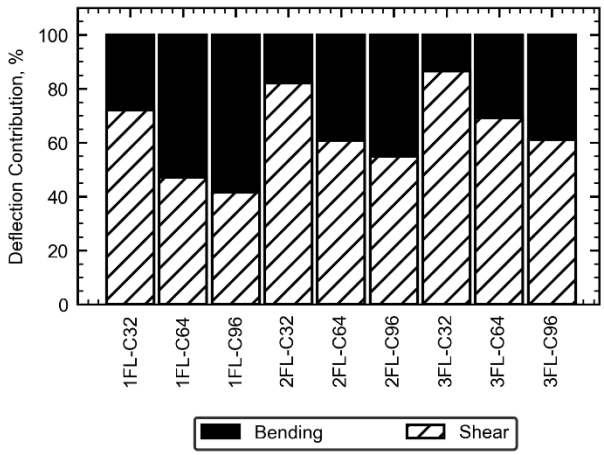

46

47 **Figure 14. Average deflection contribution from shear and bending predicted by NIIM**

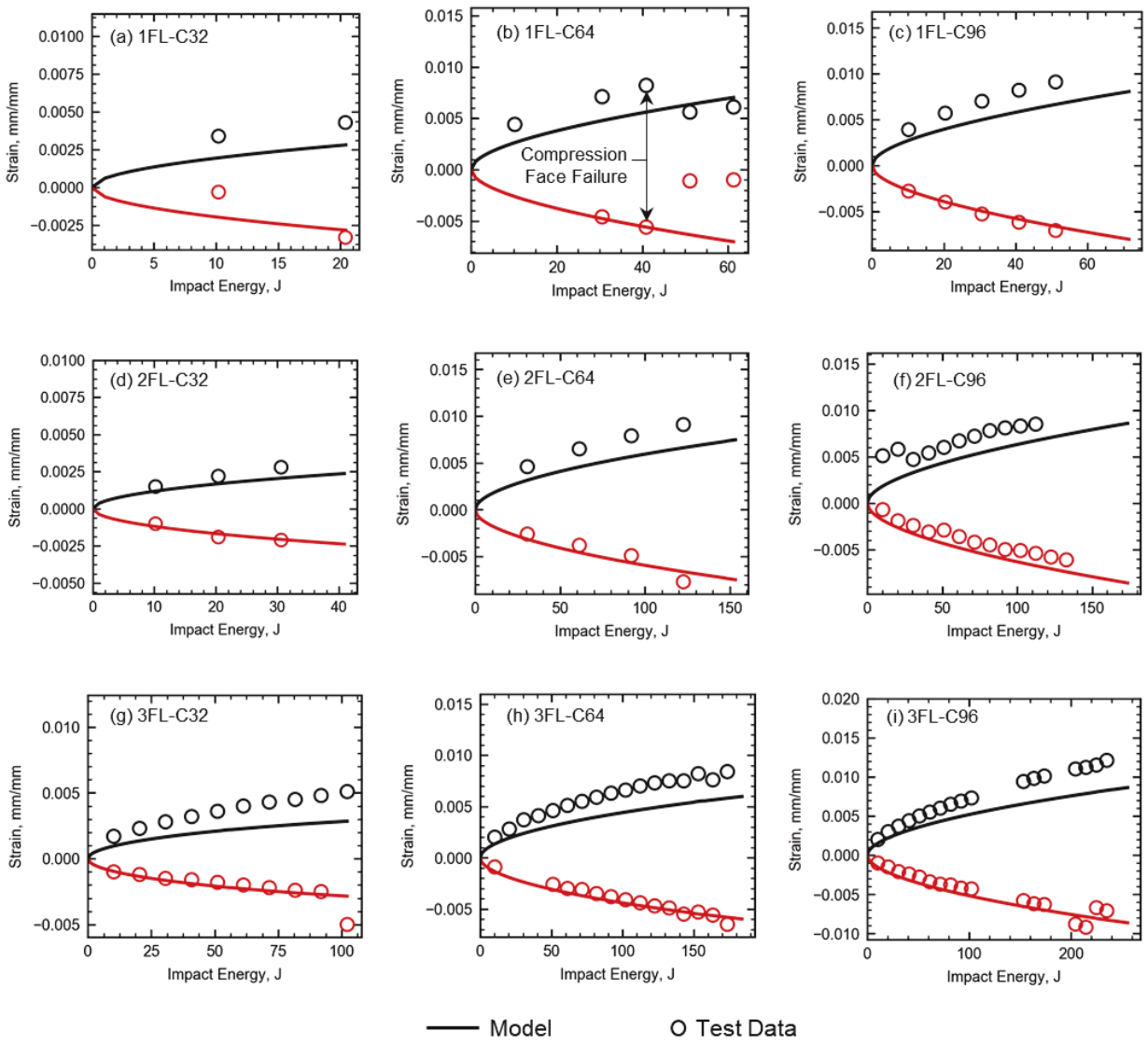

Figure 15. Verification of mid-span face strain model (top face strains are negative; bottom face strains are positive): (a) 1FL-C32; (b) 1FL-C64; (c) 1FL-C96; (d) 2FL-C32; (e) 2FL-C64; (f) 2FL-C96; (g) 3FL-C32; (h) 3FL-C64; and (i) 3FL-C96